Transport Phenomena and Conduction Mechanism of Individual Cross-Junction SnO_2 Nanobelts

*Zheng Guo, Xing Chen, Jin-Huai Liu, and Xing-Jiu Huang**

In the past several decades, nanodevices and nanoelectronics have been received great attention owing to their potential applications in many fields. Various functional nanodevices fabricated with individual one-dimensional nanostructures have been widely investigated.[1–3] Nowadays, accompanied with the development of current nanoelectronics, complex structured nanodevices and nanosystems have also been gradually involved into the scope of scientists' research interests, and further developed for achieving novel functionalities based on directly prepared hierarchical nanostructures or assembled nanostructures with one-dimensional nanostructures.[4,5]

Recently, many novel nanodevices fabricated with as-synthesized various complex nanostructures have been reported. For example, Y-shaped carbon nanotube has been prepared and used as logic switches.[4] Tetra-pods ZnO has been employed to fabricate an optical sensing device with multi-channel responses.[6] In our group, individual T-shaped SnO_2 nanowire has been constructed as a current splitter.[7] Additionally, through assembling complex nanostructures with simple one-dimensional nanostructures, many logic circuits and functional nanosystems have also been successfully developed. Earlier in 2000, McEuen and coworkers reported the electrical properties of junctions consisting of two crossed single-walled carbon nanotube (SWNT) and demonstrated that a good rectifier could be fabricated with the cross junction of SWNT.[8] Since then, cross junctions consisted of other carbon nanomaterials including multi-wall carbon nanotube, single-wall carbon nanotube and graphene have been widely studied in the experiments and theories.[9–17] Their electrical properties could be also derived to various electronic functional units. Furthermore, Lieber and coworkers have been addressing the research of nanoelectronics from logic gates to decoders of integrated nanosystems through assembling Si and Ge nanowires to form crossbar structure.[18–20] And now they have successfully developed programmable nanowire circuits for nanoprocessors.[5] Among the reported complex structured nanodevices, great interests has been mainly focused on the junction structures, especially for cross-junction (crossbar) architecture because it could be employed as a fundamental unit to construct sensing device, dense logic and memory circuits, which displays a great potential application in the future nanoelectronics.[21–24] As mentioned above, many cross-junction nanodevices have been widely performed in nanoelectronics. However, they mainly focused on the studies of Si, Ge and carbon nanomaterials.

As is well-known, metal oxide nanomaterials such as SnO_2, ZnO, In_2O_3, etc are of great importance in various fields, especially for nanosensors and electronic nanodevices.[25–30] However, till now most of the reported researches have been paid attention to individual or numerous one-dimensional nanostructure nanodevices.[31–34] To the best of our investigation, few researches about cross-junction nanodevice assembled with metal oxide nanostructures have been reported.[35] Here SnO_2 nanobelts, as a typical semiconductor metal oxide, have been firstly employed to fabricate individual cross-junction nanodevice via a nanomanipulation method as one of promising approaches to manipulate various nanostructures. Then their electrical characteristics have been investigated in details. Furthermore the corresponding model and mechanism have also been proposed to clarify the novel electrical properties arising from the cross-junction point. We believe that this novel cross-junction nanodevice based on SnO_2 nanobelts could be potentially applied as sensors with a good sensing performance.

Through a typical synthesis (see the Experimental Section of Supporting Information),[36] large scale of SnO_2 nanobelts have been obtained, which has been confirmed from the characterization results of scanning electron microscopy (SEM), transmission electron microscopy (TEM) and X-ray diffraction (XRD). (see Supporting Information, Figure S1) Then, based on the S100 Zyvex manipulator system, two nanobelts have been transferred to the SiO_2/Si substrate and successfully fabricated a cross-junction structure between them, as shown in **Figure 1**. Firstly, SnO_2 nanobelts have been dispersed onto Si wafer with microchannels. Afterwards, a single SnO_2 nanobelt has been selected and transferred to the center space of four Au/Ti electrodes via nanoprobes equipped on the manipulator, which is presented in Figure 1a. Then another nanobelt has been also transferred to the same position. However, in order to obtain a cross-junction structure between two SnO_2

Dr. Z. Guo, Dr. X. Chen, Prof. J. H. Liu,
Prof. X. J. Huang
Research Center for Biomimetic Functional Materials and Sensing Devices
Institute of Intelligent Machines
Chinese Academy of Sciences
Hefei, 230031, PR China
E-mail: xingjiuhuang@iim.ac.cn

DOI: 10.1002/smll.201200672

© 2013 Wiley-VCH Verlag GmbH & Co. KGaA, Weinheim

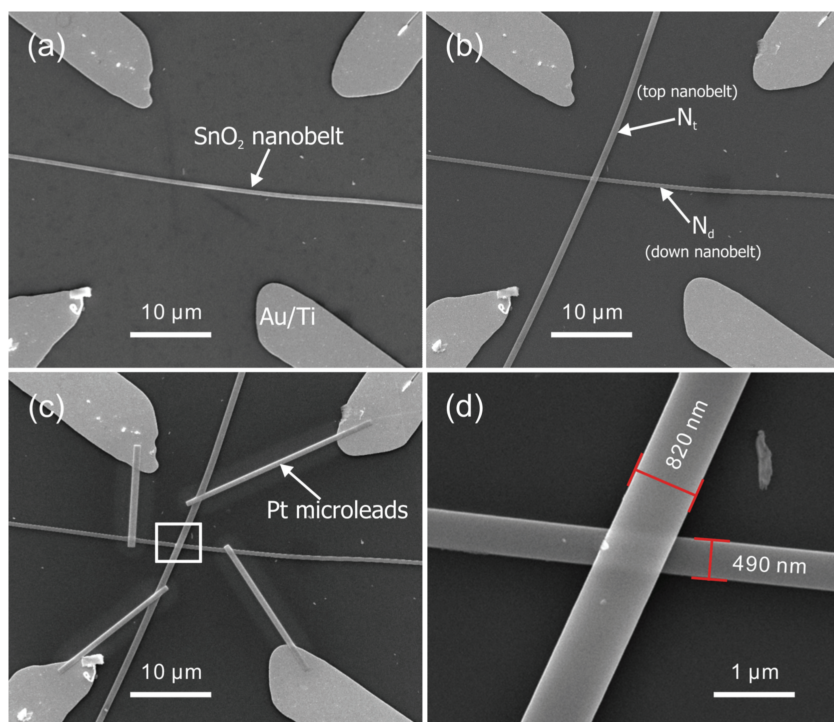

Figure 1. SEM images of main processes for the fabrication of cross-junction nanodevice with two SnO_2 nanobelts: (a) single SnO_2 nanobelt transferring to the SiO_2/Si substrate with four Au/Ti electrodes, (b) the cross junction structure constructed with two SnO_2 nanobelts fabricated with nanomanipulator, (c) the fabricated cross-junction nanodevice and (d) high magnified SEM image corresponding to the square area in (c).

nanobelts, the specific position of the other one should be carefully manipulated and gradually placed on the Si wafer substrate, which makes two SnO_2 nanobelts closely contact and finally form a cross-junction structure. Figure 1b presents SEM image of the final morphology for the cross junction consisted of two SnO_2 nanobelts. (More details about the process of fabrication, see Supporting Information, Figure S2) Afterwards, a FIB approach has been employed to deposit Platinum microleads, which connects four Au/Ti electrodes with each terminal of two SnO_2 nanobelts, respectively. The fabricated individual cross-junction nanodevice is shown in Figure 1c. Figure 1d is the magnified SEM image corresponding to the white square area at the cross junction presented in Figure 1c. Evidently, it could be observed that two SnO_2 nanobelts closely contact. For the bottom (**N_d**) and the top nanobelt (**N_t**), the width is about 490 and 820 nm, respectively.

In order to further confirm the thickness of two nanobelts for the cross-junction device, an AFM approach has been implemented. As presented in **Figure 2**a, it could be easily observed that the morphologies of SnO_2 nanostructures are real nanobelts. Figure 2b shows the scanning height along the green line presented in Figure 2a. Relative to the substrate, it can be concluded that the height is about 50 nm, which corresponds to the thickness of bottom SnO_2 nanobelt. For the top one, its thickness is about 150 nm, which could be inferred from the black line displayed in Figure 2c. Additionally, the red line along the cross junction is also performed, as shown in Figure 2d. Obviously the height is about 200 nm, which is consistent with the sum of the thickness of the top and bottom nanobelts. So it is further demonstrated that the formed cross-junction SnO_2 nanobelts closely intercontact. Combined with their width shown in Figure 1d, the ratios of width to thickness for the top nanobelt and the bottom one are about 5 and 10, respectively.

In the following, the electrical properties of the fabricated cross-junction two SnO_2 nanobelts have been systematically investigated. Firstly, their I–V characteristics have been performed for the ***a-b**, **c-d*** and ***a-d*** terminals shown in the left-top inset of **Figure 3**a, which are along the top, bottom nanobelts and across the cross-junction point, respectively. The measured results have been described in Figure 3a. According to the red I-V curve of *a-b* terminals for the top nanobelt and the blue one corresponding to ***c-d*** terminals of the bottom nanobelt, it is clear that both of them are quasi-linear at the bias voltage ranging from –2 to 2 V, indicating that there is a good ohmic contact between the deposited Pt microleads and SnO_2 nanobelts. Combining with the geometric parameters (length, width and thickness), the resistivity of two nanobelts could be further obtained from their I-V curves. It is about 3.40 Ω·cm for the top nanobelt and 4.49 Ω·cm for the bottom nanobelt, which is approximately consistent with those of the stem and branch of T-shaped SnO_2.[7] This result is also agreement with 3.01 Ω·cm of the resistivity for SnO_2 nanowire recently reported by Luo et al.[37] However, I-V curve

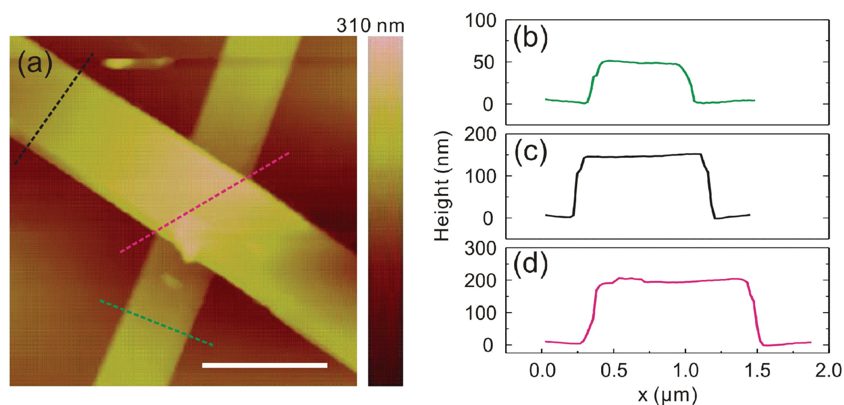

Figure 2. (a) AFM image of cross-junction SnO_2 nanobelts for the fabricated device; (b), (c) and (d) the height of bottom nanobelt, top nanobelt and cross junction relative to the substrate, respectively. Scale bar, 1 μm.

© 2013 Wiley-VCH Verlag GmbH & Co. KGaA, Weinheim

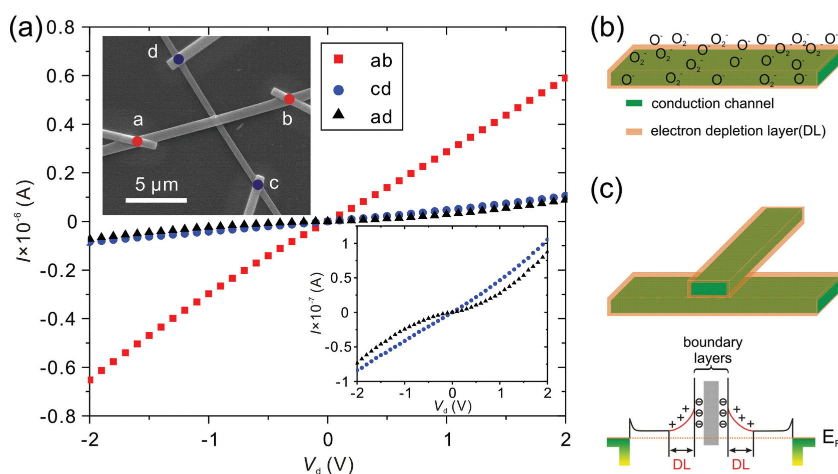

Figure 3. (a) I-V curves for the cross-junction nanodevice fabricated with two SnO_2 nanobelts. The red, blue and black lines correspond to the measurement approach of ***a-b***, ***c-d*** and ***a-d*** terminals, respectively. The left-top inset corresponding to the approach of measurement; the right-bottom inset corresponding to the magnification of I–V curves of ***c-d*** and ***a-d*** terminals. (b) Scheme of electron depletion layer and conduction channel for SnO_2 nanobelts exposed in air and (c) Energy band diagrams for the fabricated cross junction consisted of two SnO_2 nanobelts.

corresponding to the black line is not linear for ***a-d*** terminals across the cross-junction point, which is evidently demonstrated in the right-bottom inset of Figure 3a. Furthermore, for other two terminals cross-junction point including ***a-c***, ***b-c*** and ***b-d*** their I–V curves also present similar results, which are not shown here. Undoubtedly, this kind of I-V characteristic is arised from the cross-junction point. As is well-known, SnO_2, as a typical sensing material of semiconductor metal oxide, can easily interact with oxygen molecular in air leading to the formation of O^- and O_2^- on its surface.[38] So an electron depletion layer will be formed around SnO_2 nanobelts, as presented in Figure 3b. Accordingly its electron transport mainly depends on the conduction channel covered with electron depletion layer for individual nanobelt.[1,39] However, electron transport across the cross-junction SnO_2 nanobelts would be blocked by electron depletion layers. In addition, it should be noted that there is still an infinitely small gap between two nanobelts at the cross junction although they closely contact. Hence, electron transport across the cross junction should overcome the potential barrier arising from electron depletion layer between two nanobelts and an infinitely small gap at the cross-junction point,[28,40] as shown in Figure 3c. This is the reason that the I–V curves of any two terminals across the cross junction show nonlinear characteristics.

Enlightened by multi-terminals of the fabricated cross-junction structure similar with individual T-junction SnO_2 nanowire, a measurement approach analogous to the operation of field effect transistor has been also performed. As described in **Figure 4**a, two terminals of ***a*** and ***b*** for top nanobelt are used as drain and source, respectively; the c terminal for bottom nanobelt is employed as 'gate'. The corresponding equivalent circuit is also similar with the case of T-junction SnO_2 device (see supporting information, Figure S3). As shown in Figure 4b, the source–drain current I_d increases linearly with the increasing of source–drain voltage V_d under the constant 'gate' voltage V_g. Additionally, I_d-V_d curves also shift with the change of V_g. This result indicates that the current flowing through the top nanobelt is tunable and controllable via one terminal of the bottom nanobelt without the need of an external gate. However, its electronic tunability is different from the case of T-shaped SnO_2 nanowire.[7] For the cross-junction device consisted of two SnO_2 nanobelts, the displacement of I_d-V_d curves is not proportional with the increase of V_g. When V_g is at ± 5 V, the displacements of I_d-V_d curves are both very small and closely near to the initial one under

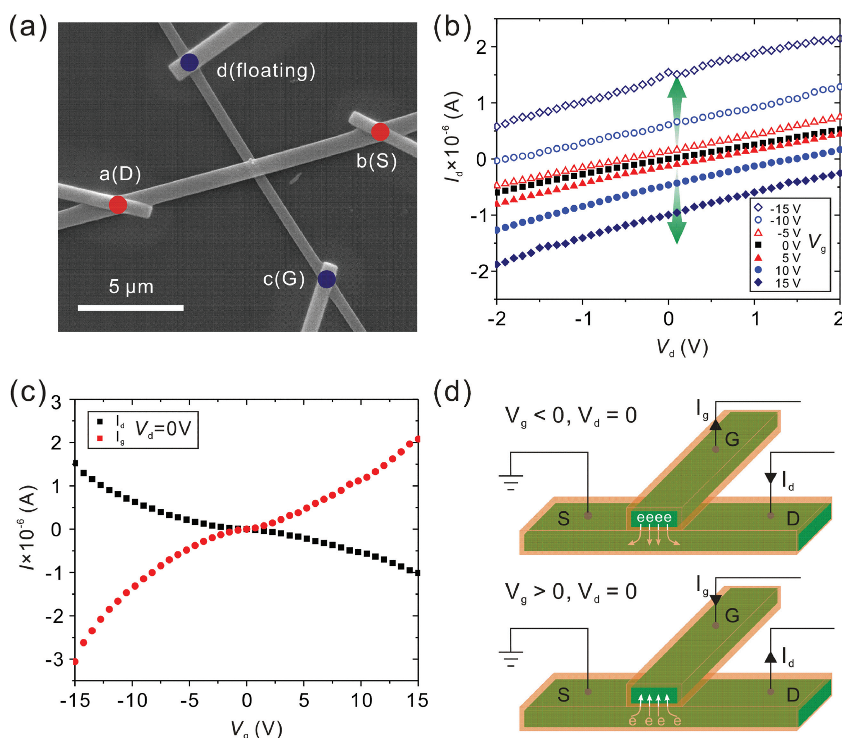

Figure 4. I-V characteristics taken on three terminals of cross-junction nanodevice constructed with two SnO_2 nanobelts. (a) Measurement approach of gating effect for cross-junction nanodevice using ***b*** as source, ***a*** as drain and ***c*** as 'gate'. (b) I_d-V_d curves under different 'gate' voltages. (c) I_d-V_g and I_g-V_g curves under V_d = 0 V. (d) The flowing direction of I_g and I_d for Vg < 0 V and > 0 V at V_d = 0 V.

© 2013 Wiley-VCH Verlag GmbH & Co. KGaA, Weinheim

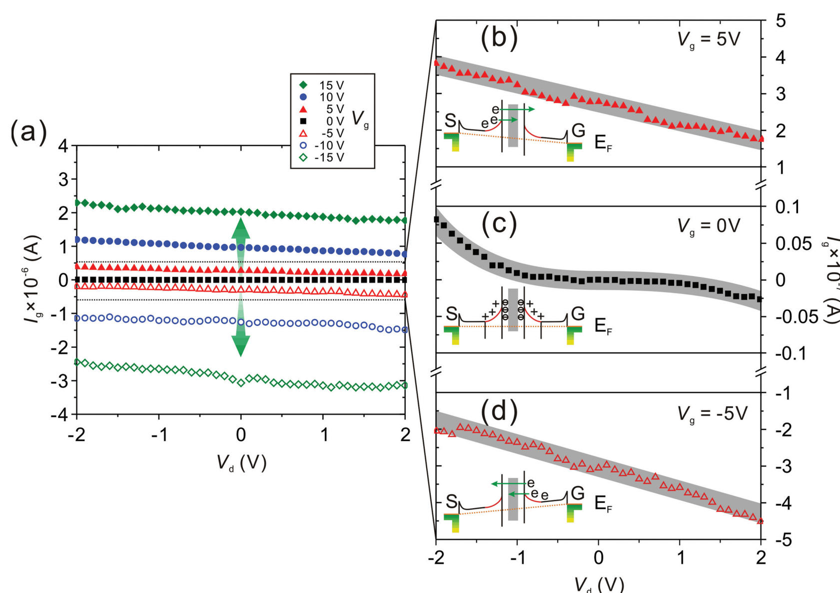

Figure 5. (a) I_g-V_d curves under different 'gate' voltages. (b), (c) and (d) the curves corresponding to under V_g = 5, 0 and –5 V, respectively. The insets of (b), (c), and (d) corresponding to energy band diagrams induced by electron field under V_g > 0, = 0 and < 0 V, respectively.

V_g = 0 V. For the gate voltage of ±10 V, it could be clearly observed that I_d –V_d curves have been gradually deviated from the initial curve. Increasing to ± 15 V, much more large displacements have been displayed. This phenomenon can be further confirmed from the nonlinear characteristic curve of I_d-V_g under V_d = 0 V, which is the black one presented in Figure 4c. It could be found that the absolute increment of I_d is gradually amplified with the 'gate' voltage deviated from 0 V. Furthermore, I_g increases with the increase of V_g and their relationship is also nonlinear based on the red one shown in Figure 4c. Figure 4d shows the flowing direction of I_g and I_d for Vg < 0 V and > 0 V at V_d = 0 V. Compared with the case of T-junction SnO_2 nanowire, we believe that the above results could be ascribed to the native physical property of the cross junction.

In **Figure 5**, the non-proportional displacement of I_g–V_d curves with V_g has also been demonstrated. And the absolute increment of its displacement turns larger and larger with the 'gate' voltage gradually deviated from 0 V, as shown in Figure 5a. This result is indirectly confirmed from the relationship between I_g and V_g under the fixed V_d = 0 V shown in Figure 4c. It is also easily observed that I_g decreases with the increase of V_d under the constant 'gate' voltage V_g. For the measurement approach of cross-junction nanodevice analogous to the operation of FET, even though there is a potential barrier at the cross-junction point, the gate is still not a perfect insulting gate, easily leading that a leakage current would be diverted from one path to the other one across the cross junction. When the 'gate' terminal has not been applied by a bias voltage (V_g = 0 V), obviously the potential barrier between two nanobelts keeps its native physical state, as shown in the inset of Figure 5c. With a source–drain voltage applied, I_g of the leakage current following through the cross-junction point will depend on the effects of tunneling and thermionic emission of electron. Accordingly, under V_g = 0 V, the relationship between I_g and V_d is nonlinear, as shown in Figure 5c. However, under the 'gate' voltage of ±5 V, two I_g-V_d curves are approximately linear, as displayed in Figure 5b and d. This tendency of I_g–V_d curves from nonlinear to quasi-linear has been further demonstrated in **Figure 6**. Actually, the potential barrier at the cross junction cannot be regarded as a constant. When a bias voltage either positive or negative is applied at the 'gate' terminal, it will be weakened attributing to the introduction of electron field, which are shown in the insets of Figure 5b and d, respectively.[40,41] Obviously, compared with the initial state without a bias voltage electrons will have much more possibility to cross the potential barrier, leading to the increase of leakage current. At a low bias voltage, the effect of potential barrier is still obvious although the leakage current increases. So, the relationship between the leakage current and the source–drain voltage is still nonlinear under the 'gate' voltage less than ±5 V. However, at a high bias voltage more than ±5 V the current following the cross junction will be dominated by the leakage current. Hence, I_g-V_d curves are cline to be linear. Based on the above analysis, the non-proportional displacement of I_d-V_d and I_g-V_d curves with V_g has also been clarified, which are shown in Figure 4b and 5a, respectively. Moreover, it can be concluded that the absolute value of the leakage current will also be larger at a higher bias voltage. That is to say, the source–drain and 'gate' currents present an amplified effect through manipulating the potential barrier at the cross junction. Hence, based on this tunable mechanism combining with a like-FET measurement approach, this cross-junction device with multi-terminals could be further employed as a sensor. Besides interacting with SnO_2 nanobelts, the analytes also interact with the cross junction, affecting its potential barrier. Through monitoring the source–drain and 'gate' currents, the sensing response would be amplified besides multi-channel response signal, which will enhance the selectivity and sensitivity.[6] Furthermore, this case can be extended to fabricate homo- or heterogeneous cross junction consisted of other metal oxide nanostructures.

Similar results have also been demonstrated for the following measurement approach using *c* as source, *d* as drain and *a* as 'gate' (see Supporting Information, Figure S4). The measurement results indicate that the source–drain current is also observed to linearly increase when the source–drain voltage is increased under the constant 'gate' voltage. Additionally, the gate current is also observed to decrease with the increasing of source–drain voltage. As expectedly, the displacement of I_d-V_d and I_g-V_d curves present similar results that they wouldn't be proportionally shifted accompanying with the gate voltage gradually deviated from 0 V. Moreover, under the 'gate' voltage V_g = 0 V, the relationship between I_g and V_d still show a nonlinear curve, which is consistent with

© 2013 Wiley-VCH Verlag GmbH & Co. KGaA, Weinheim

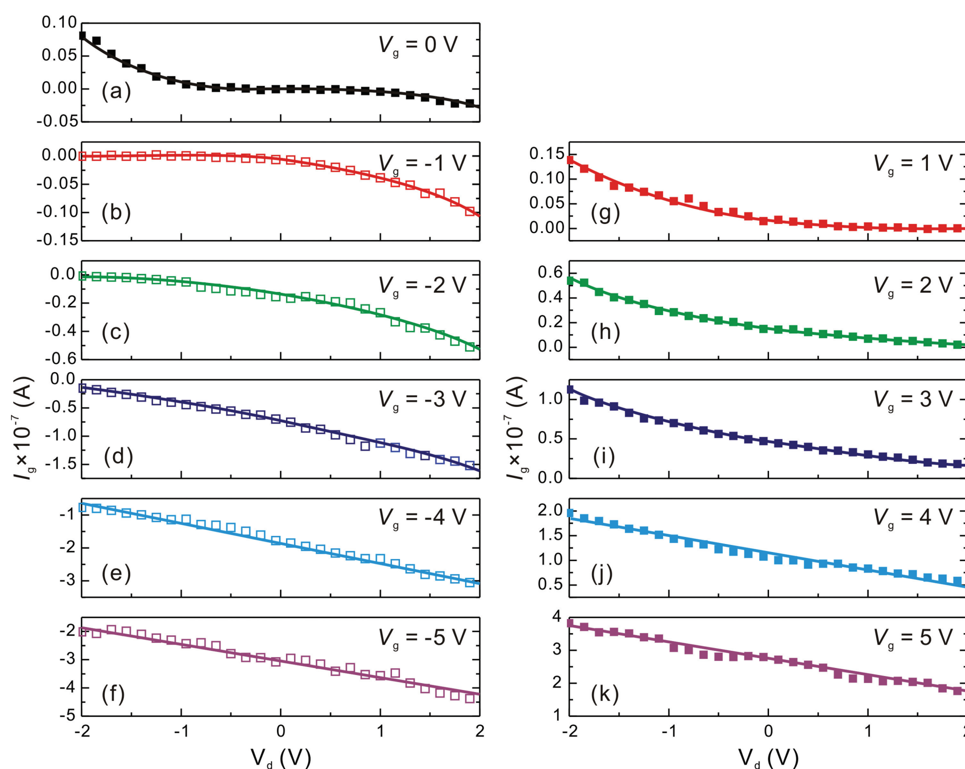

Figure 6. For measurement approach of gating effect for the cross junction using ***b*** as source, ***a*** as drain and ***c*** as 'gate'. (a) - (k) I_g-V_d curves corresponding to under V_g = 0, −1, −2, −3, −4, −5, 1, 2, 3, 4, and 5 V, respectively.

that of the former measurement approach. And with V_g deviated from 0 to ±5 V, their I_g-V_d curves also turn linear. (see Supporting Information, Figure S5)

In conclusion, electrical properties have been addressed for individual cross junction fabricated with two SnO_2 nanobelts. Owing to the electron depletion layer and an infinitely small gap at the cross-junction point, I-V curve of electron transport across the cross junction of SnO_2 nanobelts shows a nonlinear characteristics. Moreover, the current along one of two nanobelts as a source–drain channel can be manipulated by the 'gate' voltage applied on one terminal of the other nanobelt when the constant source–drain voltage is applied. Different from that of T-junction SnO_2 nanowire, the tunability of I_d-V_d and I_g-V_d characteristics is not proportionally varied with the 'gate' voltage. The absolute increment of their displacements gradually increases with the gate voltage gradually deviated from 0 V, which is attributed to the weakness of potential barrier at the cross junction induced by extra electron field. Enlightened by this phenomenon, we believe that this fabricated cross-junction device of SnO_2 nanobelts could be potentially applied as sensors. Through monitoring the source–drain and 'gate' currents, the sensing response would be amplified besides obtaining multi-channel signals, leading to enhance the selectivity and sensitivity.

Experimental Section

Synthesis and Characterization of SnO_2 Nanobelts: Concerning to synthesis of SnO_2 nanobelts, thermal evaporation method was employed according to Zhang's report.[36] More details about the synthesis process can be found in the experimental section of Supporting Information. The morphology and microscopy of the as-prepared samples were characterized by scanning electronic microscopy (FESEM, FEI Quanta 200 FEG), transmission electron microscopy (TEM, JEM-200CX). The XRD pattern of the sample was recorded on a Philips X'Pert diffractometer (XRD, X'Pert Pro MPD) with Cu Kα radiation (1.5418 Å). Atomic force microscopy (AFM) images were implemented using Nanoscope III (Digital Instruments, Veeco Metrology).

Fabrication and Electrical Measurement of Individual Cross-Junction Nanodevices: In order to fabricate individual cross junction consisted of two SnO_2 nanobelts, a S100 Zyvex manipulator system was employed, which was carried out in the Quanta 200 FEG environmental scanning electronic microscopy (ESEM). In order to improve the manipulating efficiency, Si wafer with microchannels were designed and employed to support the SnO_2 nanobelts. The main fabrication process of cross-junction structure consisted of two SnO_2 nanobelts as following: Firstly, single SnO_2 nanobelt dispersed on Si wafer with microchannels was selected through tungsten probes equipped on the nanomanipulator and transferred to the central of an Au/Ti electrode array fabricated by photolithography on a thermally grown SiO_2 layer with a thickness of 500 nm. Afterwards, the other one was also be selected and transferred to the same space and carefully put it on the substrate leading to form a cross junction with the first SnO_2 nanobelt. Then via a focused ion beam (FIB) system with SEM capability (Dual-Beam 235 FIB system from FEI Company), platinum microleads were deposited on each terminal of cross-junction two SnO_2 nanobelts, and connected with the Au/Ti electrodes.

© 2013 Wiley-VCH Verlag GmbH & Co. KGaA, Weinheim

The electrical characterization of the cross-junction nanodevice was also investigated via the manipulator system processing four independent heads equipped with tungsten probes. A Keithley 4200 semiconductor characterization system (Keithley 4200-SCS) was employed to apply the voltage and measure the current from each terminal of cross-junction two SnO_2 nanobelts. The details about all measurements could be found in our previous report.[7]

Supporting Information

Supporting Information is available from the Wiley Online Library or from the author.

Acknowledgements

This work was supported by the National Natural Science Foundation of China (61106012, 61102013, 21073197, 50901073, and 90923033), and the One Hundred Person Project of the Chinese Academy of Sciences, China. The authors acknowledge Dr. Qiang Luo and Dr. Hai-Fang Yang, the Laboratory of Microfabrication, Institute of Physics, CAS, for their experimental assistance.

[1] M. Law, H. Kind, B. Messer, F. Kim, P. D. Yang, *Angew. Chem.-Int. Ed.* **2002**, *41*, 2405.
[2] Y. Cheng, P. Xiong, C. S. Yun, G. F. Strouse, J. P. Zheng, R. S. Yang, Z. L. Wang, *Nano Lett.* **2008**, *8*, 4179.
[3] T. Y. Wei, P. H. Yeh, S. Y. Lu, Z. Lin-Wang, *J. Am. Chem. Soc.* **2009**, *131*, 17690.
[4] P. R. Bandaru, C. Daraio, S. Jin, A. M. Rao, *Nat. Mater.* **2005**, *4*, 663.
[5] H. Yan, H. S. Choe, S. W. Nam, Y. J. Hu, S. Das, J. F. Klemic, J. C. Ellenbogen, C. M. Lieber, *Nature* **2011**, *470*, 240.
[6] Z. X. Zhang, L. F. Sun, Y. C. Zhao, Z. Liu, D. F. Liu, L. Cao, B. S. Zou, W. Y. Zhou, C. Z. Gu, S. S. Xie, *Nano Lett.* **2008**, *8*, 652.
[7] Z. Guo, X. Chen, W. H. Xu, J. Li, G. M. Yang, M. Q. Li, J. H. Liu, X. J. Huang, *Mater. Today* **2011**, *14*, 42.
[8] M. S. Fuhrer, J. Nygard, L. Shih, M. Forero, Y. G. Yoon, M. S. C. Mazzoni, H. J. Choi, J. Ihm, S. G. Louie, A. Zettl, P. L. McEuen, *Science* **2000**, *288*, 494.
[9] A. Arun, P. Salet, A. M. Ionescu, *J. Nanosci. Nanotechnol.* **2011**, *11*, 4919.
[10] F. A. Bulat, L. Couchman, W. T. Yang, *Nano Lett.* **2009**, *9*, 1759.
[11] L. Y. Jiao, X. J. Xian, Z. Y. Wu, J. Zhang, Z. F. Liu, *Nano Lett.* **2009**, *9*, 205.
[12] D. S. Lee, J. Svensson, S. W. Lee, Y. W. Park, E. E. B. Campbell, *J. Nanosci. Nanotechnol.* **2006**, *6*, 1325.
[13] E. J. H. Lee, K. Balasubramanian, M. Burghard, K. Kern, *Adv. Mater.* **2009**, *21*, 2720.
[14] D. H. Kim, J. Huang, H. K. Shin, S. Roy, W. Choi, *Nano Lett.* **2006**, *6*, 2821.
[15] T. Pei, H. T. Xu, Z. Y. Zhang, Z. X. Wang, Y. Liu, Y. Li, S. Wang, L. M. Peng, *Appl. Phys. Lett.* **2011**, *99*, 113102.
[16] N. Yoneya, K. Tsukagoshi, Y. Aoyagi, *Appl. Phys. Lett.* **2002**, *81*, 2250.
[17] Q. Qing, D. A. Nezich, J. Kong, Z. Y. Wu, Z. F. Liu, *Nano Lett.* **2010**, *10*, 4715.
[18] Y. J. Dong, G. H. Yu, M. C. McAlpine, W. Lu, C. M. Lieber, *Nano Lett.* **2008**, *8*, 386.
[19] G. H. Yu, C. M. Lieber, *Pure Appl. Chem.* **2010**, *82*, 2295.
[20] Z. H. Zhong, D. L. Wang, Y. Cui, M. W. Bockrath, C. M. Lieber, *Science* **2003**, *302*, 1377.
[21] Q. X. Tang, Y. H. Tong, W. P. Hu, Q. Wan, T. Bjornholm, *Adv. Mater.* **2009**, *21*, 4234.
[22] Y. Chen, G. Y. Jung, D. A. A. Ohlberg, X. M. Li, D. R. Stewart, J. O. Jeppesen, K. A. Nielsen, J. F. Stoddart, R. S. Williams, *Nanotechnology* **2003**, *14*, 462.
[23] G. Snider, P. Kuekes, R. S. Williams, *Nanotechnology* **2004**, *15*, 881.
[24] J. W. Han, J. H. Ahn, M. W. Kim, J. O. Lee, J. B. Yoon, Y. K. Choi, *Small* **2010**, *6*, 1197.
[25] H. K. Chang, F. N. Ishikawa, R. Zhang, R. Datar, R. J. Cote, M. E. Thompson, C. W. Zhou, *ACS Nano* **2011**, *5*, 9883.
[26] C. Sun, N. Mathews, M. R. Zheng, C. H. Sow, L. H. Wong, S. G. Mhaisalkar, *J. Phys. Chem. C* **2010**, *114*, 1331.
[27] G. Shin, M. Y. Bae, H. J. Lee, S. K. Hong, C. H. Yoon, G. Zi, J. A. Rogers, J. S. Ha, *ACS Nano* **2011**, *5*, 10009.
[28] A. Menzel, K. Subannajui, F. Guder, D. Moser, O. Paul, M. Zacharias, *Adv. Funct. Mater.* **2011**, *21*, 4342.
[29] Z. Guo, J. Y. Liu, Y. Jia, X. Chen, F. L. Meng, M. Q. Li, J. H. Liu, *Nanotechnology* **2008**, *19*, 345704.
[30] F. N. Ishikawa, M. Curreli, H. K. Chang, P. C. Chen, R. Zhang, R. J. Cote, M. E. Thompson, C. W. Zhou, *ACS Nano* **2009**, *3*, 3969.
[31] Y. F. Hu, Y. L. Chang, P. Fei, R. L. Snyder, Z. L. Wang, *ACS Nano* **2010**, *4*, 1234.
[32] Z. L. Wang, *J. Nanosci. Nanotechnol.* **2008**, *8*, 27.
[33] E. Comini, G. Sberveglieri, *Mater. Today* **2010**, *13*, 28.
[34] E. Comini, G. Faglia, G. Sberveglieri, Z. W. Pan, Z. L. Wang, *Appl. Phys. Lett.* **2002**, *81*, 1869.
[35] C. Cagli, F. Nardi, B. Harteneck, Z. K. Tan, Y. G. Zhang, D. Ielmini, *Small* **2011**, *7*, 2899.
[36] S. H. Sun, G. W. Meng, Y. W. Wang, T. Gao, M. G. Zhang, Y. T. Tian, X. S. Peng, L. D. Zhang, *Appl. Phys. A—Mater. Sci. Proc.* **2003**, *76*, 287.
[37] L. B. Luo, F. X. Liang, J. S. Jie, *Nanotechnology* **2011**, 22, 485701.
[38] A. Gurlo, *ChemPhysChem* **2006**, *7*, 2041.
[39] C. C. Li, Z. F. Du, L. M. Li, H. C. Yu, Q. Wan, T. H. Wang, *Appl. Phys. Lett.* **2007**, 91, 032101.
[40] J. H. Lim, H. J. Ji, G. E. Jung, K. H. Chung, G. T. Kim, J. S. Ha, J. Y. Park, S. J. Kahng, *Solid-State Electron.* **2009**, *53*, 320.
[41] S. V. Kalinin, J. Shin, S. Jesse, D. Geohegan, A. P. Baddorf, Y. Lilach, M. Moskovits, A. Kolmakov, *J. Appl. Phys.* **2005**, 98, 044503.

Received: March 28, 2012
Published online: March 19, 2013

© 2013 Wiley-VCH Verlag GmbH & Co. KGaA, Weinheim